Published by Institute of Physics Publishing for SISSA

Received: *November 2, 2005*
Revised: *December 7, 2005*
Accepted: *December 8, 2005*
Published: *January 12, 2006*

Topology with dynamical overlap fermions

Győző I. Egri,[a,b] **Zoltan Fodor,**[a,b] **Sandor D. Katz**[a] **and Kalman K. Szabó**[b]

[a] *Institute for Theoretical Physics, Eötvös University*
Budapest, Hungary
[b] *Department of Physics, University of Wuppertal*
Germany
E-mail: egri@bodri.elte.hu, fodor@bodri.elte.hu, sandor.katz@desy.de, szaboka@general.elte.hu

Abstract: We perform dynamical QCD simulations with $n_f = 2$ overlap fermions by hybrid Monte-Carlo method on 6^4 to $8^3 \times 16$ lattices. We study the problem of topological sector changing. A new method is proposed which works without topological sector changes. We use this new method to determine the topological susceptibility at various quark masses.

Keywords: Lattice QCD, Lattice Gauge Field Theories.

JHEP01(2006)049

Contents

1. Introduction

The overlap operator [1, 2] , gives a theoretically sound solution of the chirality problem on the lattice. It satisfies the Ginsparg-Wilson relation [3, 4], which ensures the exact chiral symmetry at finite lattice spacing for the propagators [5] and for the fermion action [6]. Moreover the difference in the number of left and right handed zero modes of Ginsparg-Wilson fermions can be taken as a definition of the topological charge (Q) which gives the correct result in the continuum limit [7].

However, the numerical implementation of dynamical overlap fermions is still a great challenge today (for early studies with dynamical overlap fermions we refer to [8 – 10]). The presence of nested conjugate gradients for the inversion of the Dirac operator makes the simulations considerably slower than simulations with Wilson fermions. Furthermore one has to face the non-continuity of the fermion determinant at the boundary of topological sectors. This additional difficulty can be treated exactly in frame of the Hybrid Monte Carlo (HMC) algorithm by modifying the molecular dynamics trajectory at the boundary [11]. Clearly the crossing rate between different topological sectors is heavily affected by this modification. Inappropriate treatment might confine the system into a certain topological sector which yields an unacceptably large autocorrelation time for Q in the simulation.

A few exploratory studies are already available in QCD with dynamical overlap fermions [12, 11, 13 – 16]. All handle the modification of the trajectory at the boundary in a similar style. The original proposal of [11] is modified in [14] in such a way that the acceptance rate is increased. It is shown in [15], that the introduction of several pseudofermion fields which approximate the fermion determinant, can enhance the crossing rate. The relation between the pseudofermionic (over)estimation and rare topological sector changes[1] was pointed out in [16].

[1] In the staggered formulation there was already a concern that the pseudofermion estimator obstruct the change of topological charge [17].

In this paper we study the problem of changing topological sectors in the case of the overlap operator with $n_f = 2$ fermions in dynamical HMC simulations. Section 2 will give a short introduction to the sector changing problem for overlap fermions (by summarizing and extending the work of [16]), and answers the question why the present treatment is unlikely to change Q. In section 3 a new measurement method of expectation values is proposed, which circumvents the crossing problem entirely by making simulations constrained to fixed topological sectors. In section 4 we present numerical results using the new measurement method. In section 5 conclusions are given.

2. Topological sector changing problem

After introducing pseudofermion fields [18], our partition function reads:

$$Z = \int [dU] e^{-S_g} \det H^2 = \int [dU][d\phi^\dagger][d\phi] e^{-S_g - \phi^\dagger H^{-2} \phi}, \tag{2.1}$$

where H is the hermitian overlap operator:

$$H = \left(1 - \frac{m}{2m_0}\right) H_0 + \gamma_5 m, \tag{2.2}$$

with H_0 being the massless hermitian overlap operator:

$$H_0 = m_0[\gamma_5 + \mathrm{sgn}(H_W)]. \tag{2.3}$$

Here H_W is the standard Wilson operator with negative mass $-m_0$. The sgn function in H_0 causes a Dirac-δ type singularity in the equation of motion of the momenta of the link variables. The δ-function gives a contribution whenever an eigenvalue λ of H_W changes sign. This subspace of the configuration space coincide with topological sector boundaries. The reason for this is that in the case of the overlap operator the topological charge is [5]:

$$Q = \frac{1}{2m_0} \mathrm{Tr}(H_0) = \frac{1}{2} \sum_i \mathrm{sgn}(\lambda_i) \tag{2.4}$$

This means, that there are potential walls, non-differentiable steps in the action at the topological sector boundaries. The reflection-refraction method suggested in [11] handles these potential walls correctly. Let's denote the momenta by p and the normal vector of the topological sector boundary by n. According to this method one has to modify the momenta, when arriving at a potential wall:

$$p \to \begin{cases} p - n\langle n,p\rangle + n\langle n,p\rangle \sqrt{1 - 2\frac{\Delta S}{\langle n,p\rangle^2}}, & \text{if } \langle n,p\rangle^2 > 2\Delta S \text{ (refraction)} \\ p - 2n\langle n,p\rangle, & \text{if } \langle n,p\rangle^2 < 2\Delta S \text{ (reflection)} \end{cases} \tag{2.5}$$

Thus the trajectory will go through the topological sector boundary only if $\langle n,p\rangle^2 > 2\Delta S$. In a HMC algorithm $\langle n,p\rangle = \mathcal{O}(1)$ and has exponential distribution. ΔS, however, is not the exact value of the height of the potential wall, but it is the change of the pseudofermionic action at the boundary. From now on, we will distinguish between these two quantities. We call the former $\Delta S_{\mathrm{exact}}$ and the latter ΔS_{pf}.

Let us take a closer look[2] on the relation between $\Delta S_{\rm exact}$ and $\langle \Delta S_{\rm pf} \rangle$. In particular, we show that the jump in the pseudofermionic action overestimates $\Delta S_{\rm exact}$. Let us assume that the trajectory crosses the boundary. Let H_- and H_+ be the overlap operator evaluated on the two sides of the boundary right before and after the crossing, respectively. Clearly H_- and H_+ contain the same gauge configuration, but they differ, since one eigenvalue of H_W changes sign on the boundary. In the HMC algorithm one chooses the pseudofermion field as

$$\phi = H_- \eta, \qquad \phi^\dagger = \eta^\dagger H_-,$$

where $\eta, \eta^\dagger$ are random vectors with gaussian distribution, in order to generate $\phi, \phi^\dagger$ with the correct distribution. (In a real simulation one chooses new pseudofermion configurations only at the beginning of each trajectory, but for simplicity let's consider, that ϕ and $\phi^\dagger$ are refreshed when hitting the boundary.) The jump of the pseudofermionic action now reads:

$$\Delta S_{\rm pf} = S_{\rm pf+} - S_{\rm pf-} = \eta^\dagger (H_- H_+^{-2} H_- - 1)\eta$$

The relation between $\Delta S_{\rm exact}$ and $\Delta S_{\rm pf}$ can be obtained by the following straightforward calculation:

$$\begin{aligned} e^{-\Delta S_{\rm exact}} &= \frac{\det H_+^2}{\det H_-^2} = \frac{\int [d\eta^\dagger][d\eta] e^{-\eta^\dagger \eta} e^{-\eta^\dagger (H_- H_+^{-2} H_- - 1)\eta}}{\int [d\eta^\dagger][d\eta] e^{-\eta^\dagger \eta}} = \\ &= \langle e^{-\eta^\dagger (H_- H_+^{-2} H_- - 1)\eta} \rangle_{\eta^\dagger \eta} \geq e^{-\langle \eta^\dagger (H_- H_+^{-2} H_- - 1)\eta \rangle_{\eta^\dagger \eta}} = e^{-\langle \Delta S_{\rm pf} \rangle} \end{aligned}$$

The inequality in the second line is a consequence of the concavity of the e^{-x} function. So we conclude to:

$$\langle \Delta S_{\rm pf} \rangle \geq \Delta S_{\rm exact}.$$

We can examine this relation in realistic simulations, if we take into account, that there is a simple relation between H_+ and H_-. Let's denote by λ_0 the eigenvalue of H_W which crosses zero at the boundary, and by $|0\rangle$ the eigenvector belonging to λ_0. With this notation:

$$H_+ = H_- + c|0\rangle\langle 0|,$$

where

$$c = \Delta {\rm sgn} \lambda_0 \; m_0 (1 - \frac{m}{2m_0}),$$

with $\Delta {\rm sgn} \lambda_0 = \pm 2$ being the jump of ${\rm sgn}\lambda_0$ on the boundary. The expectation value of the discontinuity in the pseudofermionic action is:

$$\begin{aligned} \langle \Delta S_{\rm pf} \rangle &= \langle \eta^\dagger (H_- H_+^{-2} H_- - 1)\eta \rangle_{\eta^\dagger \eta} \\ &= {\rm Tr}(H_- H_+^{-2} H_- - 1) \\ &= {\rm Tr}\left((1 - c|0\rangle\langle 0| H_+^{-1})(1 - c\, H_+^{-1}|0\rangle\langle 0|) - 1 \right) \\ &= -2c\langle 0|H_+^{-1}|0\rangle + c^2 \langle 0|H_+^{-2}|0\rangle. \end{aligned}$$

[2]The following considerations in this section have already partially appeared in [16].

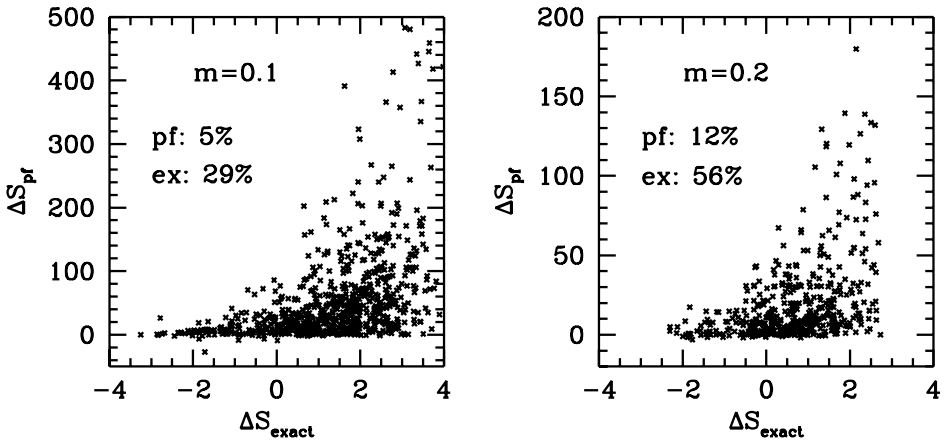

Figure 1: The jump in the exact vs. pseudofermionic action at $\beta = 4.05$ and $m = 0.1, 0.2$. Since the average of $\langle n, p\rangle^2$ is around ≈ 1, topological sector changing would happen considerably frequently using S_{exact}, than with S_{pf}. We also indicated the probability of topological sector changing with the pseudofermionic action, and an estimate on the probability using the exact action (assuming that the two algorithms would behave the same way except for the boundaries).

In a similar way one can get a simple formula for the exact value of the jump on the boundary:

$$e^{-\Delta S_{\text{exact}}} = \frac{\det H_+^2}{\det H_-^2} = \frac{1}{\det(H_+^{-1}H_-)^2} = \frac{1}{\det(1 - cH_+^{-1}|0\rangle\langle 0|)^2} = \frac{1}{(1 - c\langle 0|H_+^{-1}|0\rangle)^2}. \quad (2.6)$$

eq. (2.6) and eq. (2.6) offers a numerically fast way to determine both action jumps, since one needs only one inversion of the overlap operator to obtain both of them.

For illustration we made a scatter plot (figure 1) from a 6^4 lattice at two different masses. (Details of our action will be described in section 4.) One can clearly see, that the use of the pseudofermions has an awkward consequence: there are a huge amount of crossings, where the topological sector changing fails only due to the overestimation. One way to cure this is to use several pseudofermion estimators instead of one [15]. More pseudofermions mean smaller spread of the pseudofermionic action distribution, therefore the overestimation is smaller, too. However the computational time also increases with the number of extra fields. Obviously the best would be to use the exact action in the simulations, but only its discontinuity on the boundary can be calculated easily. The next section will present a technique, which uses this discontinuity to get the relative weight of topological sectors.

3. The new method

In this section we propose a new method for the calculation of physical observables by which it becomes possible to circumvent the problem of topological sector changing described in the previous section. Let us write the partition function in the form (assuming a vanishing

θ parameter):

$$Z = \sum_{Q=-\infty}^{\infty} Z_Q,$$

where Z_Q is the partition function of the topological sector Q. The expectation value of an observable:

$$\langle O \rangle = \frac{\sum_Q Z_Q \langle O \rangle_Q}{\sum_Q Z_Q} = \frac{\sum_Q \frac{Z_Q}{Z_0} \langle O \rangle_Q}{\sum_Q \frac{Z_Q}{Z_0}},$$

where the restricted expectation value $\langle O \rangle_Q$ is

$$\langle O \rangle_Q = \frac{1}{Z_Q} \int [dU]_Q O[U] \det H_Q^2 \exp(-S_g).$$

For reasons which will be clear later the integration goes not only over the configurations with Q charge, but also over the boundary of the topological sector as well (though the boundary has only zero measure in this case). When calculating the partition function in a given topological sector the following boundary prescription is used: we define the determinant on the boundary as the limit of determinants approaching the wall from the Q side ($\det H_Q^2$). If the measurement of the quantities Z_{Q+1}/Z_Q would be possible, then we could recover Z_Q/Z_0 for any Q. With these in hand, we would need only the restricted expectation values $\langle O \rangle_Q$, whose measurement doesn't require topological sector changings.

Now we will show a way to measure Z_{Q+1}/Z_Q. It will make use of the fact, that we can calculate easily ΔS_{exact} on the boundary of topological sectors (see eq. (2.6)). The pseudofermionic action is only used to generate configurations in fixed topological sectors, so its bad distribution for the jump of the action will not effect us. (In the following formulae ΔS will automatically mean ΔS_{exact}.) The main idea is the following: an observable measured in sector Q is inversely proportional to Z_Q and an observable in $Q+1$ is to Z_{Q+1}. If the observables in the two sectors are concentrated only to the common wall separating the two sectors, then from the ratio of the two expectation values one can recover the ratio of the two sectors.

First let us measure in the Q sector an operator, which is concentrated to the boundary:

$$\langle \delta_{Q,Q+1} F \rangle_Q = \frac{1}{Z_Q} \int [dU]_Q \delta_{Q,Q+1} F[U] \det H_Q^2 \exp(-S_g), \tag{3.1}$$

where we introduced the distribution $\delta_{Q,Q+1}$, a Dirac-δ, which is equal to zero everywhere but on the $Q, Q+1$ boundary. Then let us measure another operator G on the same wall (thus on the boundary separating sectors Q and $Q+1$), but now from the $Q+1$ sector:

$$\langle \delta_{Q,Q+1} G \rangle_{Q+1} = \frac{1}{Z_{Q+1}} \int [dU]_{Q+1} \delta_{Q,Q+1} G[U] \det H_{Q+1}^2 \exp(-S_g). \tag{3.2}$$

The wall is the same (i.e. $[dU]_Q \delta_{Q,Q+1} = [dU]_{Q+1} \delta_{Q,Q+1}$) in both cases, however due to our boundary prescription the determinants are different on it. Therefore if F and G satisfies

$$F[U] \det H_Q^2[U] = G[U] \det H_{Q+1}^2[U] \tag{3.3}$$

for configurations on the boundary, then the ratio of eq. (3.1) and eq. (3.2) gives us

$$\frac{\langle \delta_{Q,Q+1} F \rangle_Q}{\langle \delta_{Q,Q+1} G \rangle_{Q+1}} = \frac{Z_{Q+1}}{Z_Q}. \tag{3.4}$$

The easiest choice is $G(U) = 1$ and $F(U) = \det H^2_{Q+1} / \det H^2_Q = \exp(-\Delta S)$, the ratio of sectors becomes:

$$Z_{Q+1}/Z_Q = \frac{\langle \delta_{Q,Q+1} \exp(-\Delta S) \rangle_Q}{\langle \delta_{Q,Q+1} \rangle_{Q+1}}. \tag{3.5}$$

This choice is still not optimal, since the measurement of the numerator is problematic, if the distribution of ΔS extends to negative values. The exponential function amplifies the small fluctuations in the negative ΔS region, which can destroy the whole measurement: a very small fraction of the configurations will dominate the result. As a consequence one ends up with relatively large statistical uncertainties. With a slightly different choice of F and G we can improve on the situation. With $F(U) = \Theta(\Delta S - x) \exp(-\Delta S)$ and $G(U) = \Theta(\Delta S - x)$ we can omit the problematic part of the ΔS distribution (the values smaller than x) from the measurement, and we get:

$$Z_{Q+1}/Z_Q = \frac{\langle \delta_{Q,Q+1} \exp(-\Delta S) \rangle_Q^{\Delta S > x}}{\langle \delta_{Q,Q+1} \rangle_{Q+1}^{\Delta S > x}}. \tag{3.6}$$

The price of this choice of F, G is that we do not make use of the $\Delta S < x$ part of our data set. The value of x can be tuned to minimize the statistical error.

Let us note that eq. (3.3) can be viewed as a detailed balance condition on a given U configuration between Q and $Q+1$ sector (F and G are just the "transition probabilities"). This can give us a hint, that the Metropolis-step is a good a solution for F, G: $F = \min(1, \exp(-\Delta S))$ and $G = \min(1, \exp(\Delta S))$. The ratio of sectors is simply:

$$Z_{Q+1}/Z_Q = \frac{\langle \delta_{Q,Q+1} \min(1, \exp(-\Delta S)) \rangle_Q}{\langle \delta_{Q,Q+1} \min(1, \exp(\Delta S)) \rangle_{Q+1}}. \tag{3.7}$$

The inconvenient part of the distribution ($\Delta S < 0$) is cut off, however in contrast to eq. (3.6) all configurations are used to get the expectation values.

We have achieved our main goal: without making expensive topological sector changes we can obtain the ratio of sectors (see eq. (3.5), (3.6), (3.7)). The key point is to make simulations constrained to fixed topological charge, and match the results on the common boundaries of the sectors. In the next subsection we will show in the framework of HMC, how to measure an expectation value, which contains a Dirac-delta on the surface. Our proposal is that the generation of trajectories inside a sector can be done using the pseudofermionic action, we do not need there the exact action. Since no sector changing is required, the inconvenient distribution of the pseudofermionic action jump on the boundary will not effect the measurement of the ratios of sectors. The exact action is needed only on the boundary: the formulas (3.5), (3.6), (3.7) require ΔS.

It is clear that using the exact fermion action when measuring the ratio of sectors outperforms the conventional HMC, where topological sector changing is hindered by the distribution of the pseudofermionic action jump. Even in that (at the moment theoretical)

case if we were able to use the exact fermionic action in simulations, the above presented method is better in determining the ratios of topological sectors. Consider a small quark mass simulation, where a HMC using the exact fermionic action sticks into the trivial topological sector (now due to the fact, that nontrivial topologies are suppressed by the fermion determinant). If the simulation time is not long enough, then we have no information at all on the small (but nonvanishing) ratio Z_1/Z_0. However in our method this small quantity can be measured. The more we hit the wall from the two sides the more precisely we can measure Z_1/Z_0. The same argument applies to an R-type algorithm (where it is possible to use the exact ΔS jump, when crossing topological sectors [16]).

Obviously an important issue for this new method is whether topological sectors defined by the overlap charge are path-connected or not. In [19] it has been proven that abelian lattice gauge fields satisfying the admissibility condition can be classified into connected topological sectors. No result is known for non-abelian groups or non-admissible gauge fields. (Though there are some concerns on the structure of the space of non-abelian lattice gauge fields [20].) If configurations with the same Q would not be continuously connectable in sector Q, then our assumption that we make measurements on the common boundary of sectors could be violated. It could happen, that the wall sampled from sector Q does not coincide with the wall sampled from $Q+1$. Moreover the fixed sector simulations would also violate ergodicity in this case. Let us note here that the large autocorrelation time for the topological charge in the conventional pseudofermionic HMC effectively also causes the breakdown of ergodicity. In case of non-connected sectors one can cure these problems by releasing the system from a sector after a certain amount of time and closing it to another.

Expectation value of a δ-function

In a HMC simulation one determines the expectation value of an operator by calculating a sum over the measured values of the observable on N configurations, which are generated with the proper weights, by which they occur in the functional integral. In practice it is not possible to measure an operator containing a Dirac-delta on the boundary surface on these configurations, because none of them will be exactly located on it. Therefore we formulate a somewhat different measurement method, and discuss its properties. As a result one has to make measurements at those points of the trajectories, where they hit the boundary.

Let us see the details. Consider for a moment that we are able to integrate the hamiltonian equations of motion exactly. If the distribution of the gauge field, pseudofermion field and momenta was correct at the starting point of the trajectory, then it will be still correct for any of the inner points. This fact follows from energy and area conservation and reversibility. So we make no mistake if we put the inner points of the trajectory into the ensemble. We can write:

$$\langle O \rangle = \lim_{N\to\infty} \frac{1}{N} \sum_{i=1}^{N} O_i = \lim_{N\to\infty} \frac{1}{N} \sum_{i=1}^{N} \int_i O(U_t) dt = \lim_{N\to\infty} \frac{1}{N} \sum_{i=1}^{N} O_{i,i+1} \tag{3.8}$$

where t is the microcanonical time, U_t is the gauge configuration at time t, the i subscript at the integral means that the integration goes for the ith trajectory, and $O_{i,i+1}$ is thus

the average of the operator O along this trajectory. In the case of an observable, which contains a δ-function, like those in eq. (3.6) or in eq. (3.7) this reads:

$$O_{i,i+1} = \int_i dt\ o(U_t)\ \delta\left(\lambda_0(U_t)\right), \tag{3.9}$$

where it is indicated, that the δ-function depends on the gauge configuration only through the smallest absolute value eigenvalue λ_0 of H_W. If the variable of integration is changed from t to λ_0, we get:

$$O_{i,i+1} = \int d\lambda_0 \sum_j \left|\frac{dt}{d\lambda_0}\right|_{t_j,\lambda_0(U_{t_j})=0} o(U_{t_j})\delta(\lambda_0). \tag{3.10}$$

We can go further by determining the time derivative of the smallest eigenvalue:

$$\frac{d\lambda_0}{dt} = \left\langle 0|\ \mathrm{tr}\ \frac{\partial H_W}{\partial U^T}\frac{dU}{dt}|0\right\rangle \tag{3.11}$$

where, again $|0\rangle$ is the eigenvector belonging to λ_0. The trace and transpose operations are meant to be in color space. Recognizing, that with our previous notation

$$\frac{dU}{dt} = pU \qquad \text{and} \qquad \left\langle 0|U\frac{\partial H_W}{\partial U^T}|0\right\rangle = n$$

yields

$$\frac{d\lambda_0}{dt} = \langle n,p\rangle, \qquad \left|\frac{dt}{d\lambda_0}\right| = \frac{1}{|\langle n,p\rangle|}, \tag{3.12}$$

$$\langle O\rangle = \lim_{N\to\infty}\frac{1}{N}\sum_{i=1}^{N}\sum_j o(U_{t_j})\frac{1}{|\langle n,p_{t_j}\rangle|}\Bigg|_{t_j,\lambda_0(U_{t_j})=0} \tag{3.13}$$

If we put it simple, the above formula says, that since the integration is in microcanonical time, the angle and velocity by which the trajectory hits the boundary has to be taken into account.

Let us turn back to the case, when the integration of the equations of motion can be done only with finite step size integrator. The leap-frog procedure has $O(\epsilon^3)$ error per microcanonical step, which after $1/\epsilon$ steps makes the trajectory differ by $O(\epsilon^2)$ from the exact trajectory. If we can guarantee, that the modification of the trajectory at the boundary also violates the equations of motions only upto $O(\epsilon^2)$, then in the final results the errors will be proportional with $O(\sqrt{N}\epsilon^2)$. The original reflection algorithm in [11] has $O(\epsilon)$ errors, later it was improved to $O(\epsilon^2)$ in [14]. In the appendix we propose a different reflection procedure and prove that it is reversible, area-preserving and conserves the energy upto $O(\epsilon^2)$.

4. Numerical results

In the previous section we described a new method, to solve the topological sector changing problem of pseudofermionic HMC simulation. We describe here the details of the simulations, and finally give the topological susceptibility in physical units measured on 8^4 and $8^3\times 16$ lattices.

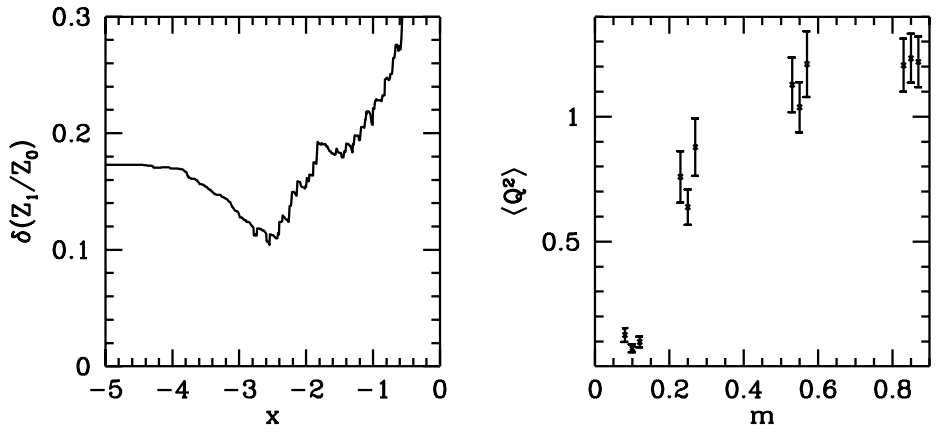

Figure 2: *Left panel:* a typical optimization procedure of the lower limit (x) on ΔS in the formula (3.6). The statistical error of the ratio Z_1/Z_0 shows a minimum as the function of x, which is considered as the optimal value. *Right panel:* Bare mass dependence of topological susceptibility using three different methods on 6^4 lattices. The points corresponding to the same mass were slightly shifted vertically for clarity. Result based on our new technique and eq. (3.6) is on the left, based on eq. (3.7) is in the middle, the standard pseudofermionic HMC is on the right. The simulation parameters are from [21]

Simulations were done using unit length trajectories, separated by momentum and pseudofermion refreshments. The system was confined to a fixed topological sector in each run, we reflected the trajectories whenever they reached a sector boundary. The end points of the trajectories obviously follow the exact distribution in a given sector, usual quantities can be measured on them. We compared a few observables (plaquette, size of the potential wall) in a given topological sector, but in different runs. We have not found any sign indicating that the sectors were disconnected. When calculating the ratio of sectors using eq. (3.5) or eq. (3.6) or eq. (3.7) we integrated along the trajectories, this quantity will be burdened by a step size error. We carried out simulations at one stepsize.

In case of large enough statistics the value of Z_{Q+1}/Z_Q should be the same, independently which of the three formula (3.5), (3.6), (3.7) was used to calculate it. We omit eq. (3.5) in the following, since it is hard to give a reliable error estimate on the expectation value of $\exp(-\Delta S)$, if ΔS can be arbitrary negative number. Eq. (3.6) still measures $\exp(-\Delta S)$, but with a lower limit (x) on ΔS. Smaller limit yields a smaller and more reliable error, however the statistics is decreased at the same time. One can tune the value of x, so that the statistical error takes its minimum. A result of a typical optimum search can be seen on the left panel of figure 2. The optimal value can be compared to the one obtained from eq. (3.7). On the right panel of figure 2 the two new topological susceptibilities and the one calculated by using traditional pseudofermionic HMC [21] are shown. The agreement is perfect. Comparing these results with those of the HMC, we conclude that the stepsize effect is negligible (at least at our present statistics). Let us compare the amount of CPU time of the two different methods for roughly the same statistical errors (see figure 2): the conventional HMC consisted 500-1000 trajectories (500 for the smallest, 1000 for the largest mass), whereas we generated less than 200 at each mass for the new

m	$\langle Q^2 \rangle$	$\langle Q^2 \rangle r_0^4/V$	r_0	m_π	Lm_π	#traj
0.03	0.13(2)	0.0047(9)	3.52(13)	0.29(11)	2.4	39
0.1	0.41(6)	0.010(1)	3.17(5)	0.53(4)	4.3	51
0.2	0.97(19)	0.017(3)	2.89(2)	0.74(6)	5.9	63
0.3	1.59(18)	0.027(3)	2.88(6)	0.99(8)	7.9	54

Table 1: Topological susceptibility measured on 8^4 lattices in the second and third column. The further columns contain the Sommer-scale, pion mass, pion mass times box size and number of trajectories on $8^3 \times 16$ lattices.

method. Moreover it is important to emphasize in this context that the new method can be efficiently parallelized.

To measure the topological susceptibility on 8^4 lattices we generated configurations with tree-level Symanzik improved gauge action ($\beta = 4.15$ gauge coupling) and 2 step stout smeared overlap kernel ($\rho = 0.15$ smearing parameter, the kernel was the standard Wilson matrix with $m_0 = 1.3$). We performed runs in sectors $Q = 0 \dots 3$ (based on the measured Z_3/Z_2 we can conclude, that the contribution of $Q \geq 4$ sectors are small compared to statistical uncertainties). For the negatively charged sectors we used the $Q \to -Q$ symmetry of the partition function. The bare masses were $m = 0.03, 0.1, 0.2$ and 0.3, at each mass approximately 1000 trajectories were collected. The average number of the topological sector boundary hittings was around 1.5 per trajectory. We calculated the ratio of sectors using eq. (3.6) and eq. (3.7). The result for the topological susceptibility can be seen on figure 3 (see also table 1). It is nicely suppressed for the smallest mass. To convert it into physical units, we made simulations on $8^3 \times 16$ lattices. We measured the static potential by fitting the large time behaviour of on and off-axis Wilson-loops. Then fitting it at intermediate distances we extracted the value of Sommer-parameter. We also measured the pion mass (see table 1). Since our statistics was quite small on these asymmetric lattices, the errors are large. Note, that in order to get the mass-dimension 4 topological susceptibility in physical units, one has to make very precise scale measurements.

When interpreting the results, one should keep in mind, that the volume is small, and the lattice spacing is large. Note however, that smeared kernel overlap actions show nice scaling behavior and good locality properties already at moderate lattice spacings [22, 23].

5. Conclusions

In this paper we studied the problem of topological sector changing in dynamical overlap simulations. The origin of the unexpectedly large autocorrelation time for the topological charge is connected to pseudofermions, which approximate the fermion determinant. The pseudofermionic action overestimates the size of the discontinuity in the fermion determinant at the topological sector boundary, so the system cannot enter easily to a new topological sector. This happens even if the use of the exact determinant favored a transition. (The discontinuity of the exact determinant can be calculated in a rather inexpensive way.)

JHEP01(2006)049

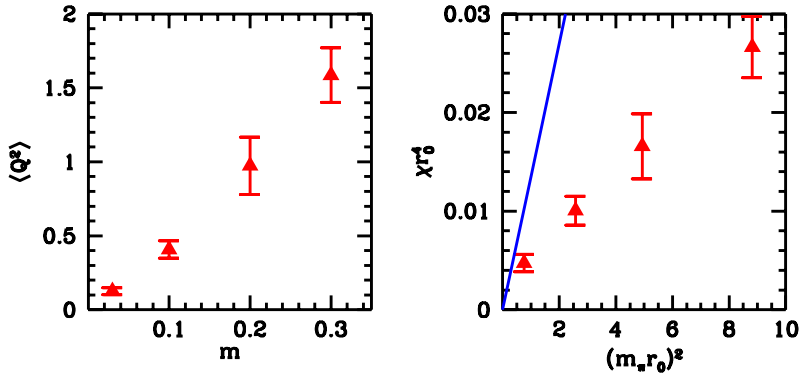

Figure 3: Topological susceptibility as the function of quark mass on 8^4 lattices in lattice units (left), and in physical units as the function of pion mass (right). Scale fixing and mass measurements were done on $8^3 \times 16$. The error bars on the right plot do not contain the errors of scale fixing. The line is the leading order chiral behavior in the continuum.

We developed a new method, which circumvents the problem of topological sector changing. It confines the system to fixed topological sectors (by always reflecting the HMC trajectories from the topological sector boundaries). Thus overestimating the discontinuity of the determinant due to pseudofermions will not effect the determination of topology related quantities. The relative weight of two topological sector is obtained by measuring appropriate operators on the common boundary surface. The measurement of such operators can be carried out by extending the usual HMC measurement method, however an $O(\epsilon^2)$ extrapolation in HMC step size is required.

The new method was tested on 6^4 lattices, where previous conventional HMC results were available. The old and new results were consistent. We also measured the topological susceptibility on 8^4 lattices with an improved overlap fermion and gauge action, furthermore simulations were done on $8^3 \times 16$ lattices to convert the lattice results into physical units.

Acknowledgments

Useful comments on the manuscript from A. D. Kennedy and discussions with T. G. Kovács are acknowledged. For this work a modified version of the MILC Collaboration's public code [24] with SSE instructions [25] was used. Simulations were carried out on the ALICENext PC-Cluster (1024 AMD-Opteron processors) at Wuppertal University, Germany and on the PC-cluster (330 Intel-P4 nodes) at the Eötvös University of Budapest, Hungary. This work was partially supported by Hungarian Scientific grants, OTKA-T34980/-T37615/M37071/T032501/AT049652. This research is part of the EU Integrated Infrastructure Initiative Hadronphyisics project under contract number RII3-CT-20040506078.

A. Appendix

We present a reflection algorithm which conserves the energy upto $O(\epsilon^2)$, and which is reversible and area conserving. Until the boundary the trajectory is evolved by the usual

leapfrog procedure. An elementary leapfrog step can be written in the following symbolic way:

$$P(\epsilon/2)U(\epsilon)P(\epsilon/2), \tag{A.1}$$

where $U(\epsilon)$ and $P(\epsilon)$ are the operators updating the links (u) and the momenta (p):

$$U(\epsilon) : u \to \exp(\epsilon p)u, \qquad P(\epsilon) : p \to p - \epsilon A\left[u\frac{\partial}{\partial u}\left(S_g + S_{\rm pf}\right)\right],$$

where in the force term the A operator projects onto traceless, antihermitian matrices (in color indices). Now we split the evolution of the links into two parts:

$$P(\epsilon/2)U(\epsilon/2)\cdot U(\epsilon/2)P(\epsilon/2). \tag{A.2}$$

Consider that the boundary would be crossed during one of the evolutions of the links in eq. (A.2). Then replace the original leapfrog with the following:

$$P(\epsilon/2)U(\epsilon/2)\cdot U(\epsilon_c)P(\epsilon_c)RP(\epsilon_c)U(\epsilon_c)\cdot U(\epsilon/2)P(\epsilon/2),$$

where R is simply the reflection of the momenta (eq. (2.5)). ϵ_c is the time to reach the boundary surface measured from the midpoint of the leapfrog. Thus if the crossing would happen in the first evolution then $\epsilon_c < 0$, if in the second, then $\epsilon_c > 0$. The reversibility can be checked easily, for the energy conservation we note that both $U(\epsilon)P(\epsilon)$ and $P(\epsilon)U(\epsilon)$ conserves the energy upto $O(\epsilon^2)$. If the evolution time does not depend on the variables, then both $U(\epsilon)$ and $P(\epsilon)$ are area conserving. The only problem arises due to the link and momenta dependence of ϵ_c. We will now show that the combined effect of the ϵ_c updates

$$U(\epsilon_c)P(\epsilon_c)RP(\epsilon_c)U(\epsilon_c) \tag{A.3}$$

is still area preserving.

For simplicity we will not carry out here the computation using the SU(3) structure, but only for a k-dimensional euclidean vectorspace (the q coordinates are k-component vectors). All features of the proof are also present in this simpler case. We have to calculate the jacobian of the following transformation

$$q'(q,p) = q + \epsilon_c p + \epsilon_c p' \qquad p'(q,p) = Rp + h.$$

$R_{ab} = \delta_{ab} - 2n_a n_b$ is the reflection operator ($a, b = 1 \ldots k$), where n_a is the normal vector of the surface. h can be expressed as $h = -\epsilon_c F - \epsilon_c RF$, where F is the force on the wall (interpreted in the sector into which we reflect back the trajectory). Since h is measured on the wall, its q and p derivatives satisfy $\partial h/\partial p = \epsilon_c \partial h/\partial q$ (see [11]). Furthermore h is orthogonal to n ($(nh) = 0$). For the q derivative of p' we introduce the matrix Z_{ab}, which contains the derivatives of the normal vector and h:

$$\frac{\partial p'_a}{\partial q_b} = Z_{ab}.$$

Using that n and h are functions of the wall coordinates, $\epsilon_c Z$ will appear in the p derivative of p':

$$\frac{\partial p'_a}{\partial p_b} = R_{ab} + \epsilon_c Z_{ab}.$$

The partial derivatives of q' are:

$$\frac{\partial q'_a}{\partial q_b} = \delta_{ab} + (p_a + p'_a)\frac{\partial \epsilon_c}{\partial q_b} + \epsilon_c \frac{\partial p'_a}{\partial q_b},$$
$$\frac{\partial q'_a}{\partial p_b} = \epsilon_c \delta_{ab} + (p_a + p'_a)\frac{\partial \epsilon_c}{\partial p_b} + \epsilon_c \frac{\partial p'_a}{\partial p_b}.$$

With the help of the following identities (see [11]):

$$\frac{\partial \epsilon_c}{\partial q_a} = -\frac{n_a}{(np)} \qquad \frac{\partial \epsilon_c}{\partial p_a} = -\epsilon_c \frac{n_a}{(np)},$$

the jacobian can be written in a hypermatrix form ($x \circ y$ has components $x_a y_b$):

$$J = \begin{pmatrix} \frac{\partial q'}{\partial q} & \frac{\partial q'}{\partial p} \\ \frac{\partial p'}{\partial q} & \frac{\partial p'}{\partial p} \end{pmatrix} = \begin{pmatrix} 1 & -2\epsilon_c Q \\ 0 & R \end{pmatrix} - \frac{1}{(np)} \begin{pmatrix} 1 & \epsilon_c \\ 0 & 0 \end{pmatrix} \otimes [(p + p') \circ n] + \begin{pmatrix} \epsilon_c & \epsilon_c^2 \\ 1 & \epsilon_c \end{pmatrix} \otimes Z.$$

Q is the projector to the subspace orthogonal to n ($Q = 1 - n \circ n$). J can be written as a product of two matrices $J = J_1 J_2$, where

$$J_1 = \begin{pmatrix} 1 & -2\epsilon_c Q \\ 0 & R \end{pmatrix},$$

having determinant -1 (since R is a reflection).

$$J_2 = \begin{pmatrix} 1 & 0 \\ 0 & 1 \end{pmatrix} \otimes 1 - \frac{1}{(np)} \begin{pmatrix} 1 & \epsilon_c \\ 0 & 0 \end{pmatrix} \otimes [(p + p') \circ n] + \begin{pmatrix} -\epsilon_c & -\epsilon_c^2 \\ 1 & \epsilon_c \end{pmatrix} \otimes RZ,$$

which has an upper triangular form in the 2×2 space in a suitable basis. The determinant of J_2 will be unity due to the orthogonality of $p + p' = p + Rp + h = -2Qp + h$ and n. Therefore $\det J = -1$, which shows that the transformation (A.3) preserves the area.

References

[1] H. Neuberger, *Exactly massless quarks on the lattice*, *Phys. Lett.* **B 417** (1998) 141 [hep-lat/9707022].

[2] H. Neuberger, *More about exactly massless quarks on the lattice*, *Phys. Lett.* **B 427** (1998) 353 [hep-lat/9801031].

[3] P.H. Ginsparg and K. G. Wilson, *A remnant of chiral symmetry on the lattice*, *Phys. Rev.* **D 25** (1982) 2649.

[4] P. Hasenfratz, *Prospects for perfect actions*, *Nucl. Phys.* **63** *(Proc. Suppl.)* (1998) 53 [hep-lat/9709110].

JHEP01(2006)049

[5] R. Narayanan and H. Neuberger, *A construction of lattice chiral gauge theories*, *Nucl. Phys.* **B 443** (1995) 305 [hep-th/9411108].

[6] M. Lüscher, *Exact chiral symmetry on the lattice and the Ginsparg-Wilson relation*, *Phys. Lett.* **B 428** (1998) 342 [hep-lat/9802011].

[7] P. Hasenfratz, V. Laliena and F. Niedermayer, *The index theorem in QCD with a finite cut-off*, *Phys. Lett.* **B 427** (1998) 125 [hep-lat/9801021].

[8] R. Narayanan, H. Neuberger and P.M. Vranas, *A simulation of the Schwinger model in the overlap formalism*, *Phys. Lett.* **B 353** (1995) 507 [hep-lat/9503013].

[9] H. Neuberger, *The overlap lattice Dirac operator and dynamical fermions*, *Phys. Rev.* **D 60** (1999) 065006 [hep-lat/9901003].

[10] A. Bode, U.M. Heller, R.G. Edwards and R. Narayanan, *First experiences with hmc for dynamical overlap fermions*, hep-lat/9912043.

[11] Z. Fodor, S.D. Katz and K.K. Szabo, *Dynamical overlap fermions, results with hybrid Monte-Carlo algorithm*, *JHEP* **08** (2004) 003 [hep-lat/0311010].

[12] G. Arnold et al., *Numerical methods for the QCD overlap operator. II: optimal Krylov subspace methods*, hep-lat/0311025.

[13] N. Cundy et al., *Numerical methods for the QCD overlap operator. III: nested iterations*, *Comput. Phys. Commun.* **165** (2005) 221 [hep-lat/0405003].

[14] N. Cundy et al., *Numerical methods for the QCD overlap operator. IV: hybrid monte carlo*, hep-lat/0502007.

[15] T. DeGrand and S. Schaefer, *Physics issues in simulations with dynamical overlap fermions*, *Phys. Rev.* **D 71** (2005) 034507 [hep-lat/0412005].

[16] T. DeGrand and S. Schaefer, *Chiral properties of two-flavor QCD in small volume and at large lattice spacing*, *Phys. Rev.* **D 72** (2005) 054503 [hep-lat/0506021].

[17] H. Dilger, *Topological zero modes in Monte Carlo simulations*, *Int. J. Mod. Phys.* **C6** (1995) 123–134 [hep-lat/9408017].

[18] S. Duane, A.D. Kennedy, B.J. Pendleton and D. Roweth, *Hybrid Monte Carlo*, *Phys. Lett.* **B 195** (1987) 216.

[19] M. Lüscher, *Abelian chiral gauge theories on the lattice with exact gauge invariance*, *Nucl. Phys.* **B 549** (1999) 295 [hep-lat/9811032].

[20] D.H. Adams, *Gauge fixing, families index theory and topological features of the space of lattice gauge fields*, *Nucl. Phys.* **B 640** (2002) 435 [hep-lat/0203014].

[21] Z. Fodor, S.D. Katz and K.K. Szabo, *Dynamical overlap fermions, results with HMC algorithm*, *Nucl. Phys.* **140** *(Proc. Suppl.)* (2005) 704 [hep-lat/0409070].

[22] T.G. Kovacs, *Locality and topology with fat link overlap actions*, *Phys. Rev.* **D 67** (2003) 094501 [hep-lat/0209125].

[23] S. Durr, C. Hoelbling and U. Wenger, *Filtered overlap: speedup, locality, kernel non-normality and Z(A) approx. 1*, *JHEP* **09** (2005) 030 [hep-lat/0506027].

[24] http://physics.indiana.edu/~sg/milc.html.

JHEP01(2006)049

[25] Z. Fodor, S.D. Katz and G. Papp, *Better than* $1/$*mflops sustained: a scalable PC-based parallel computer for lattice QCD*, *Comput. Phys. Commun.* **152** (2003) 121 [hep-lat/0202030].